Electronic Supplementary Material (ESI) for Journal of Materials Chemistry A.

Supporting Information

A Dual-confined Lithium Nucleation and Growth Design Enables Dendrite-free Lithium Metal Battery

Lun Li, ‡ Huaqiang Fu, ‡ Jinlong Yang,* Pengyan Wang, Huazhang Zhang, Xin Zhao, Zhitong Xiao, Zhenhui Liu, Zongkui Kou, Zhenbo Wang, Daping He*

1 Experimental details

Firstly, a homogeneous solution was obtained by mixing GO (15 mg mL^{-1}) and 600 mg $AgNO_3$. The resultant solution was subsequently blade casted and dried at 60 ^oC for 12 h. Subsequently, soaking the film in the 0.1 M L^{-1} vitamin C (VC) solution under water bath with a temperature of 80 ^oC for 2h. Finally, the GO/$AgNO_3$ film was calcined at 600 ^oC for 1 h with a heating rate of 5 ^oC min^{-1} under an argon flow to obtain the Ag/N-rGO film. rGO film was also synthesized by a similar procedure without the addition of $AgNO_3$.

2 Materials Characterization

The crystal phases were identified by X-ray diffraction (XRD) on a D8 Advance X-ray diffractometer with a non-monochromatic Cu Kα X-ray radiation. The morphologies were investigated by field-emission scanning electron microscopy (FESEM) on a JEOL-7100F microscope with 20 kV acceleration voltage. Transmission electron microscopy (TEM) and high-resolution TEM (HRTEM) were carried out using a JEM-2100F microscope. Elemental mappings were collected with an EDX-GENESIS 60S spectrometer. Raman spectra were measured using a Renishaw RM-1000 micro-Raman spectroscopy system. X-ray photoelectron spectroscopy (XPS) was obtained by the VG MultiLab 2000 instrument. TGA was performed using an STA-449C thermobalance and the samples were heated from room temperature to 800 °C in air with a heating rate of 5 °C min^{-1}.

3 Electrochemical Measurements

The electrochemical properties were tested using the CR2025-type coin cells assembled in a glovebox filled with pure argon. A Celgard 2400 microporous membrane was used as separator. 1.0 M LiTFSI in a liquid mixture of 1, 2-dimethoxyethane and 1, 3-dioxolane (1:1 in volume) with 1 wt% $LiNO_3$ additive was taken as the electrolyte. 35 µL electrolyte was added in each cell. For the CE and Li deposition behavior, the Ag/N-rGO, rGO and Cu foil was used as the working electrode and a Li metal was used as counter electrode. For the long-term cycling behavior and rate capability, the symmetric cell was assembled using Li@Ag/N-rGO, Li@rGO and Li@Cu as the electrode for both sides. The Li@Ag/N-rGO, Li@rGO and Li@Cu electrodes were electrochemically deposited with a Li capacity of 3 mAh cm^{-2} at 1mA cm^{-2}. The full cells were tested at voltage range of 2.3-4.0 V. Metallic Li is electrochemically deposited onto the Ag/N-rGO substrates with a capacity of 3 mAh cm^{-2} at 1mA cm^{-2} to serve as the anode of full cells. The cathode was prepared by LFP, acetylene black, and polyvinylidene fluoride with the LFP mass ratio of 91.5% mixed in N-methyl-2-pyrrolidone to form a homogeneous slurry. The slurry was then coated onto Al foil and dried at 70 ^oC for 12 h. The mass loading of LFP electrode is 1.5-2.0 mg cm^{-2}. All the electrochemical tests were carried out with a multichannel battery testing system (LAND CT2001A). The electrochemical impedance spectra (EIS) were collected with an Autolab potentiostat/galvanostat.

4 Computational details

4.1 First Principles Calculations: Density functional theory (DFT) calculations in this work were carried out using the CASTEP program on Materials Studio. The exchange-correlation effects were described by the Perdew-Burke-Ernzerhof (PBE) functional within the generalized gradient approximation (GGA) method. The core-valence interactions were accounted by the projected augmented wave (PAW) method. The energy cutoff for plane wave expansions was set to 400 eV, and the 3×3×1 Monkhorst-Pack grid k-points were selected to sample the Brillouin zone integration. The vacuum space is adopted 20 Å above the surfaces to avoid periodic interactions. The structural optimization was completed for energy and force convergence set at 1.0×10^{-5} eV and 0.03 eV $Å^{-1}$, respectively. Each model was allowed to interact with a Li ion and the binding energy is defined as Equation (1):

$$E_b = E_{total} - E_{sub} - E_{Li}$$

where E_{total}, E_{sub}, and E_{Li} are the energy of Ag/graphene-based model bound with Li^+, Ag/graphene-based model, and Li^+, respectively.

4.2 Modeling for Deposition of Lithium: The morphology of Li metal growth with Li^+ concentration distribution and current density distribution at the interface between anode and electrolyte were carried out by CMOSOL Multiphysics with a Finite Element Analysis (FEA) model. Periodic conditions are imposed on the left and right boundaries of the model. The simulation cell was 20 μm in diameter and 40 μm in height. The entire simulation process takes 3600 s; aggressive dendrite occurs on the Cu and rGO electrode over time, while the Ag/N-rGO electrode reaches flat and smooth after 50

s. The current density is 1 mA cm^{-2}, which is consistent with experimental Settings. The Li nucleus on bare Cu surface and rGO surface is composed of irregular Li peaks, while the Ag/N-rGO surface is presented with uniformly distributed semicircular Li nucleus. These two models are both establish as an ideal model and reflect the real condition to the maximum extent.

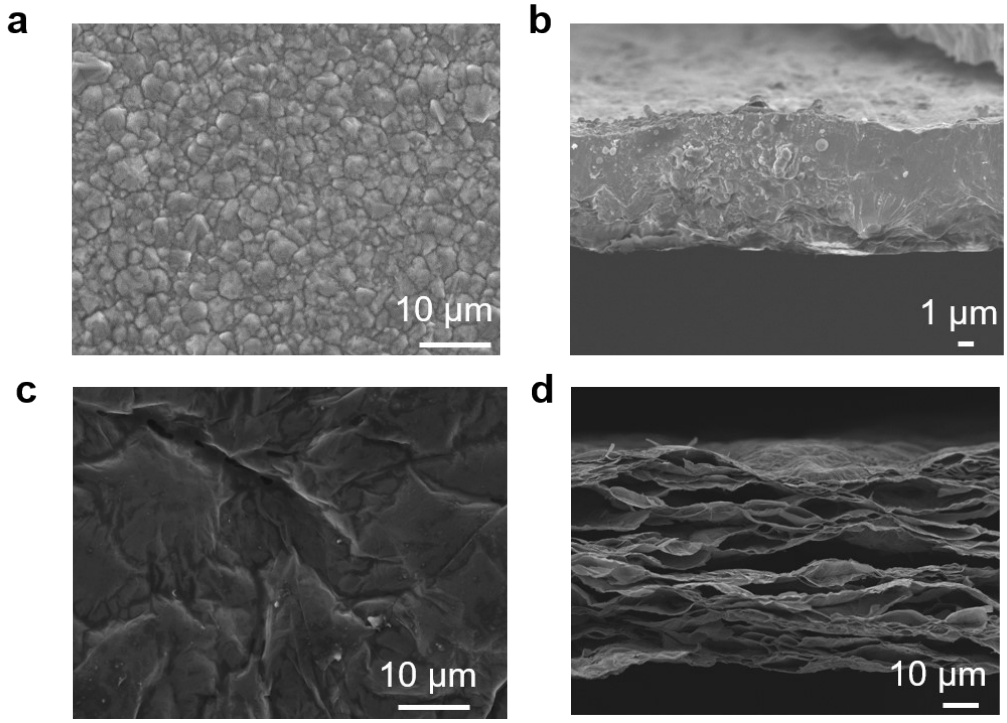

Fig. S1 Morphology characterization of bare Cu and rGO. Top view of (a) Cu, (c) rGO film. Cross-sectional view of (b) Cu, (d) rGO film.

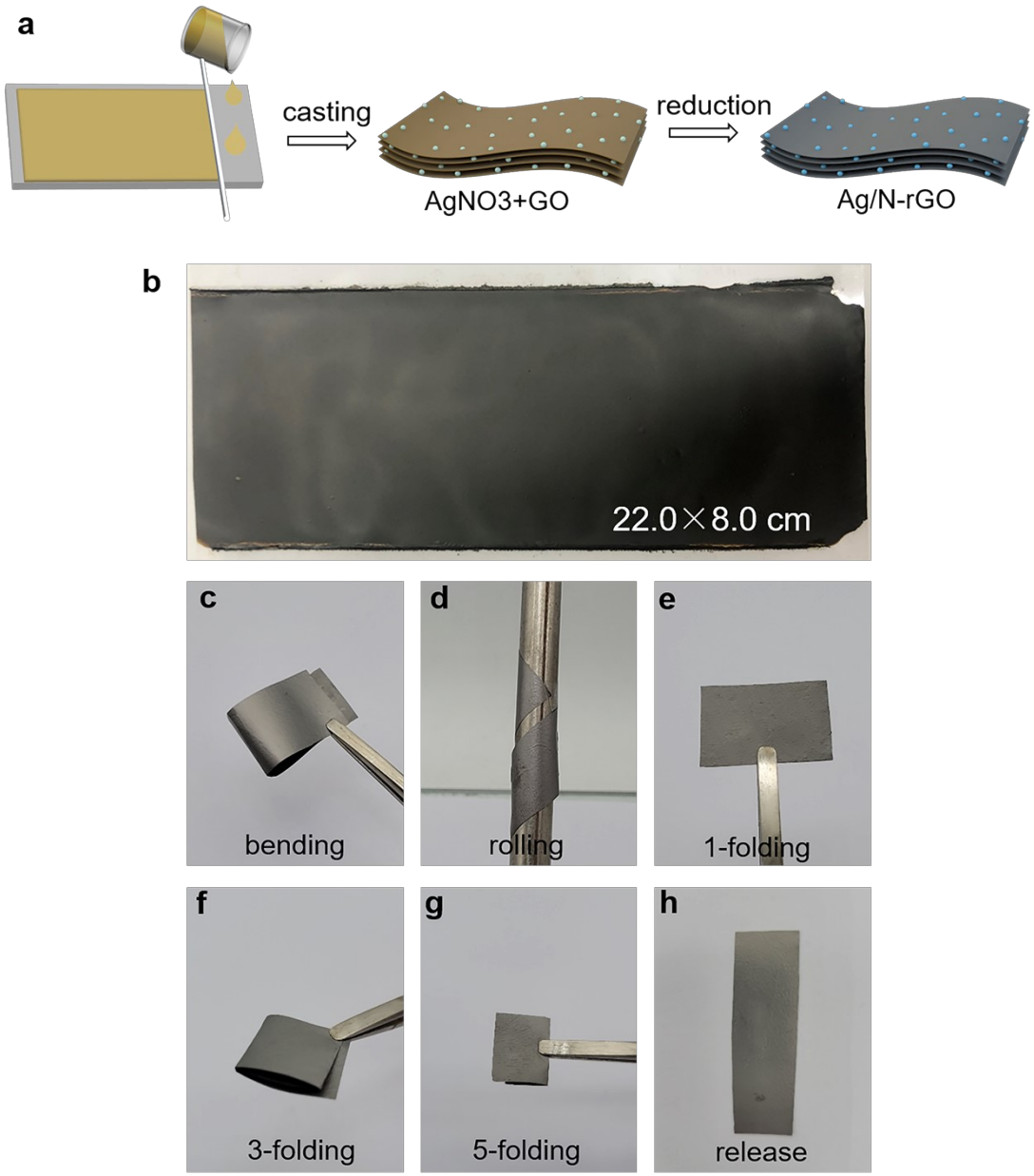

Fig. S2 Fabrication and digital photos for the appearance and flexibility of the precursor and Ag/N-rGO. (a) The synthesis procedures of Ag/N-rGO film. (b) A GO/$AgNO_3$ composite film (22.0×8.0 cm^{-2}). (c-h) Ag/N-rGO illustrating the flexibility of (c) bending, (d) rolling, (e) 1-folding, (f) 3-folding and (g) 5-folding, and (h) release.

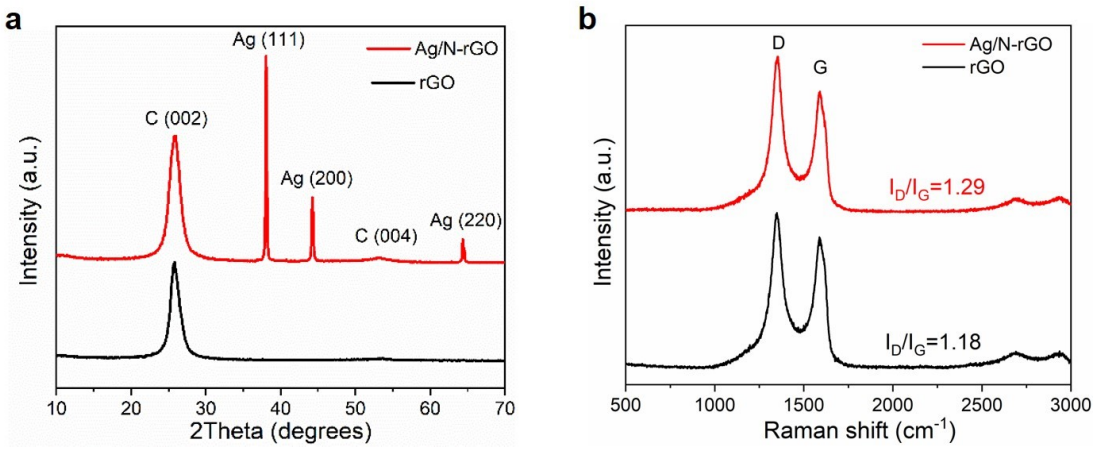

Fig. S3 Characterization of Ag/N-rGO substrate. (a) XRD patterns and (b) Raman spectra of Ag/N-rGO (red) and rGO (black).

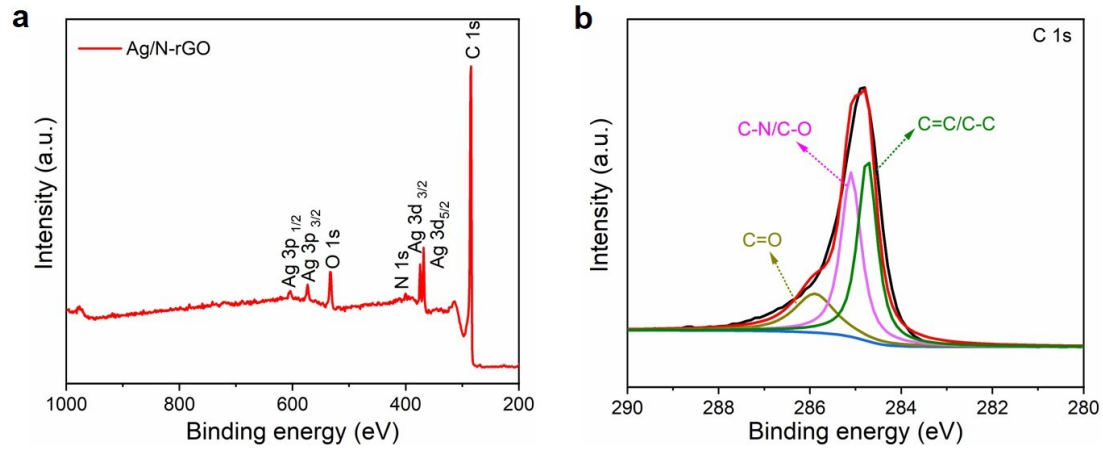

Fig. S4 Characterization of Ag/N-rGO. (a) XPS full spectra of Ag/N-rGO. (b) XPS spectra of C 1s of Ag/N-rGO.

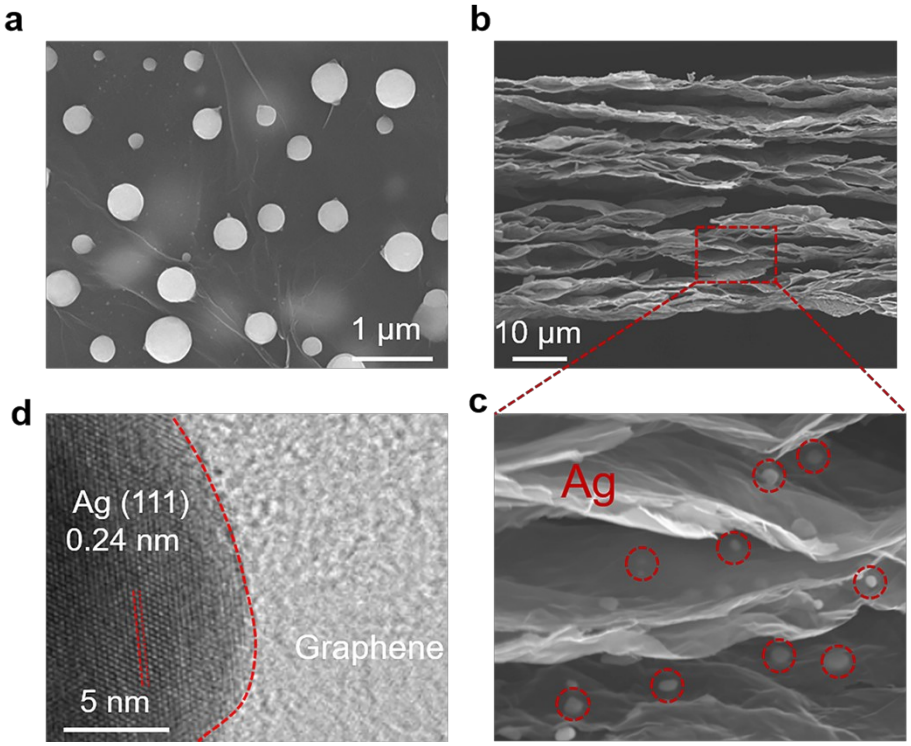

Fig. S5 Characterization of Ag/N-rGO substrate. (a) Top-view and (b-c) sectional-view SEM images of Ag/N-rGO. (d) High-resolution TEM image of Ag/N-rGO sheets.

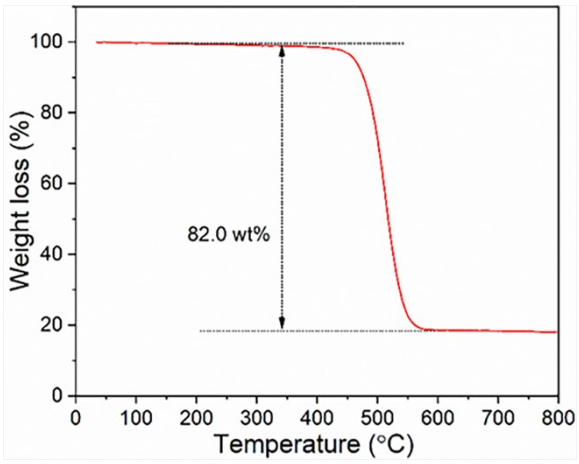

Fig. S6 Characterization of Ag/N-rGO. Thermogravimetric analysis of Ag/N-rGO in air at a heating rate of 5 ºC min^{-1}.

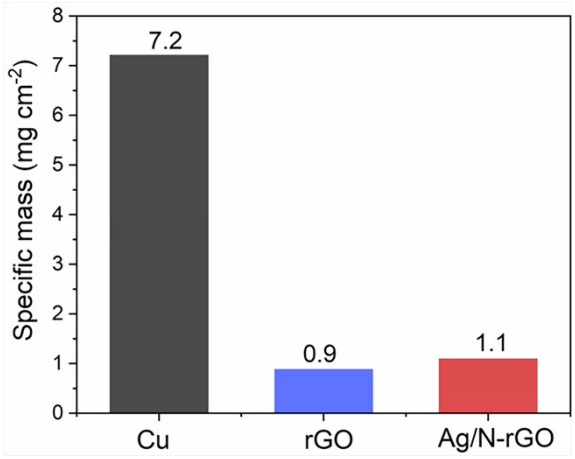

Fig. S7 Characterization of Cu, rGO and Ag/N-rGO. Specific mass of Cu, rGO and Ag/N-rGO film.

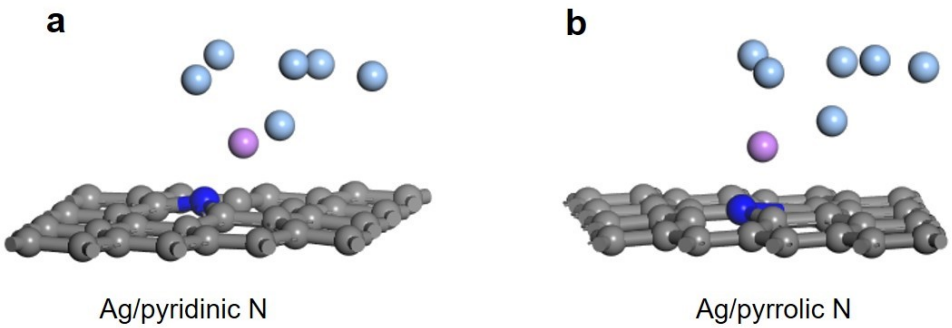

Fig. S8 DFT calculations. Optimized structure modeling of Li atom deposited on (a) Ag/pyridinic N-rGO and (b) Ag/pyrrolic N-rGO.

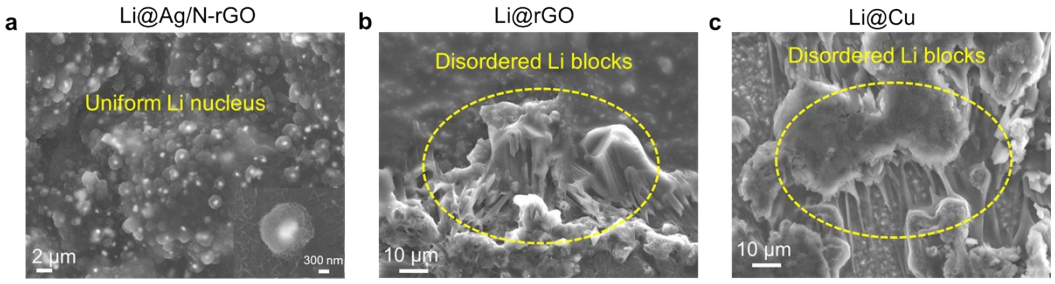

Fig. S9 Li nucleation morphology. SEM images of initial Li nucleates on the Cu, rGO and Ag/N-rGO substrate at current density of 1 mA cm^{-2} with deposition capacity of 0.2 mAh cm^{-2}.

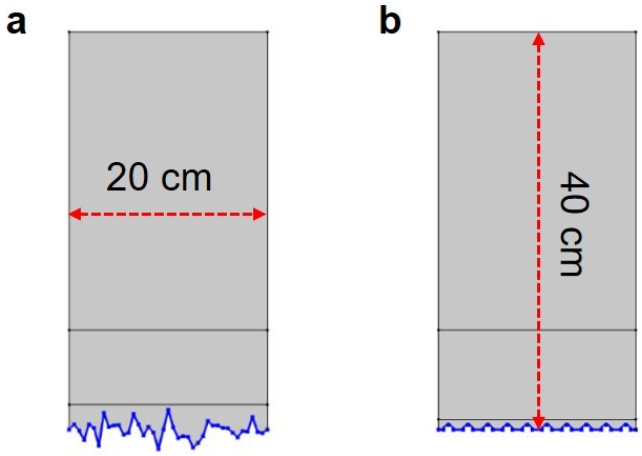

Fig. S10 COMSOL simulation details. Simulation cell geometry of initial nucleation in COMSOL for (a) Cu and rGO electrode and (b) Ag/N-rGO electrode.

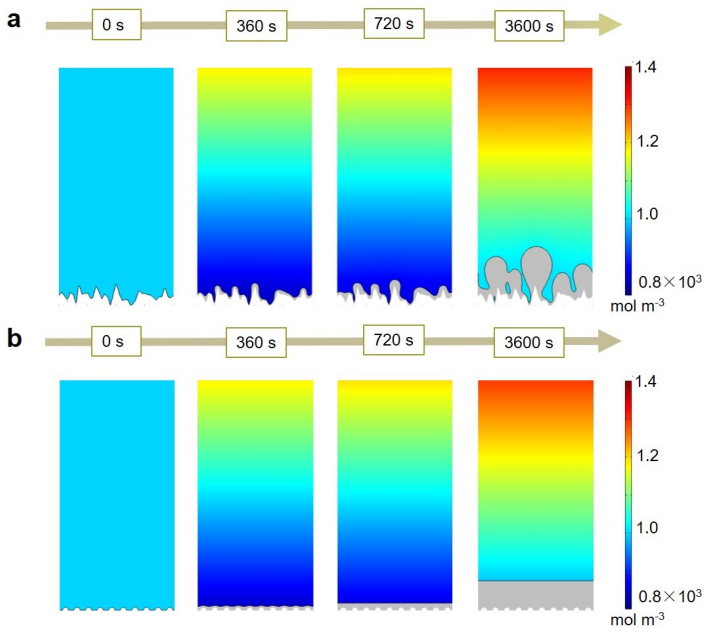

Fig. S11 COMSOL simulation results. Li^+ concentration distributions morphologies with evolution mechanism of Li metal growth under (a) randomly distributed nucleation (Cu, rGO) and (b) uniformly distributed nucleation (Ag/N-rGO).

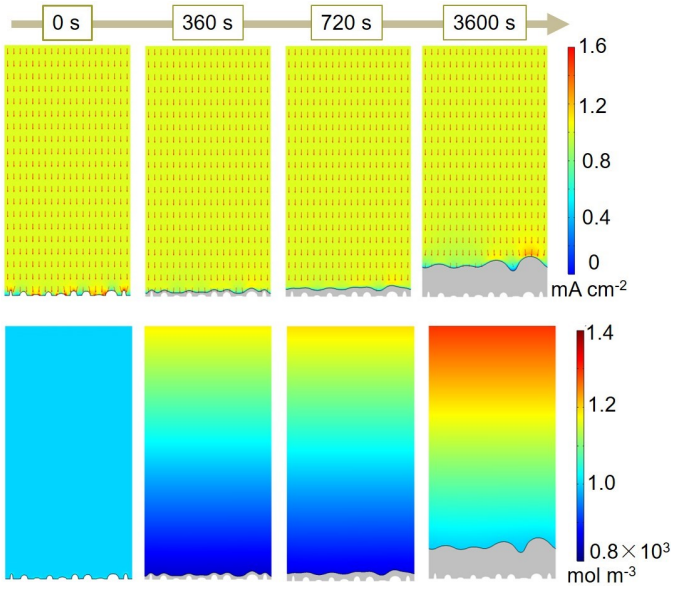

Fig. S12 COMSOL simulation results. (a) Current density distributions and (b) Li^+ concentration distributions with Li deposition morphologies evolution on N-rGO substrate.

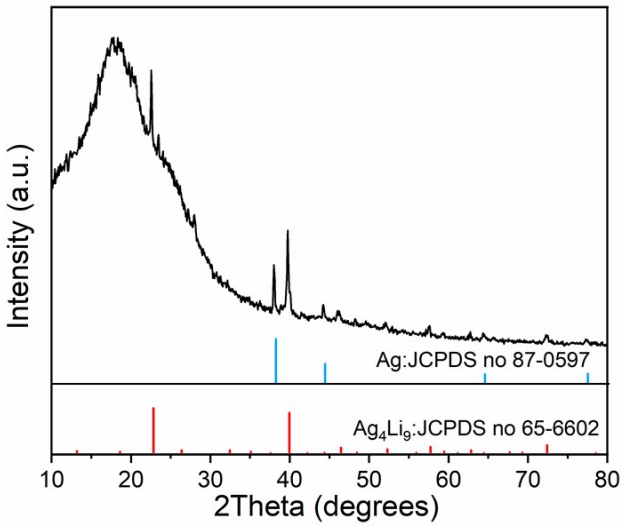

Fig. S13 Characterization of Li@Ag/N-rGO. XRD patterns of deposited Li on **Ag/N-rGO** substrate at 1 mA cm^{-2} with deposition capacity of 1 mAh cm^{-2}.

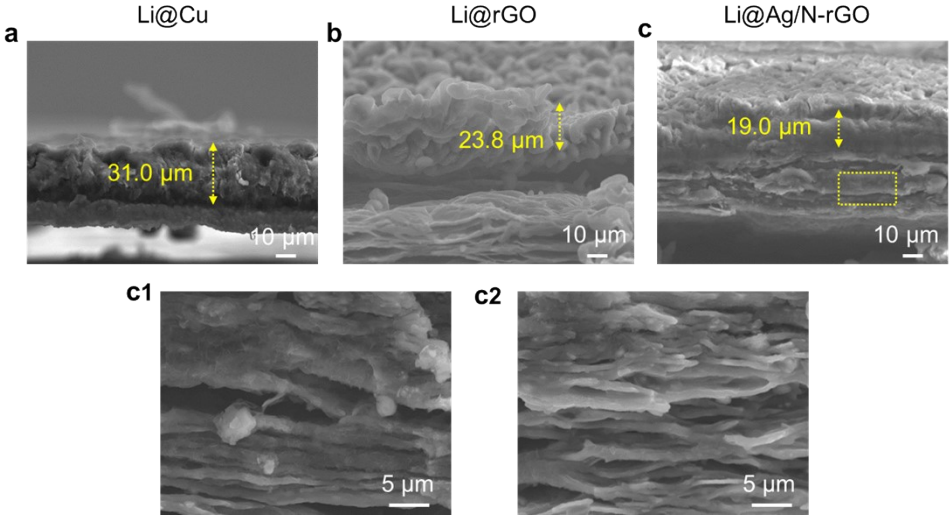

Fig. S14 Morphology of Li deposition. Cross-sectional SEM images of the Li deposition behavior on (a) Cu, (b) rGO, and (c) Ag/N-rGO substrate with a capacity of 4 mAh cm^{-2} at the current density of 1 mA cm^{-2}. (c1, c2) The enlarged cross-sectional observation of Ag/N-rGO.

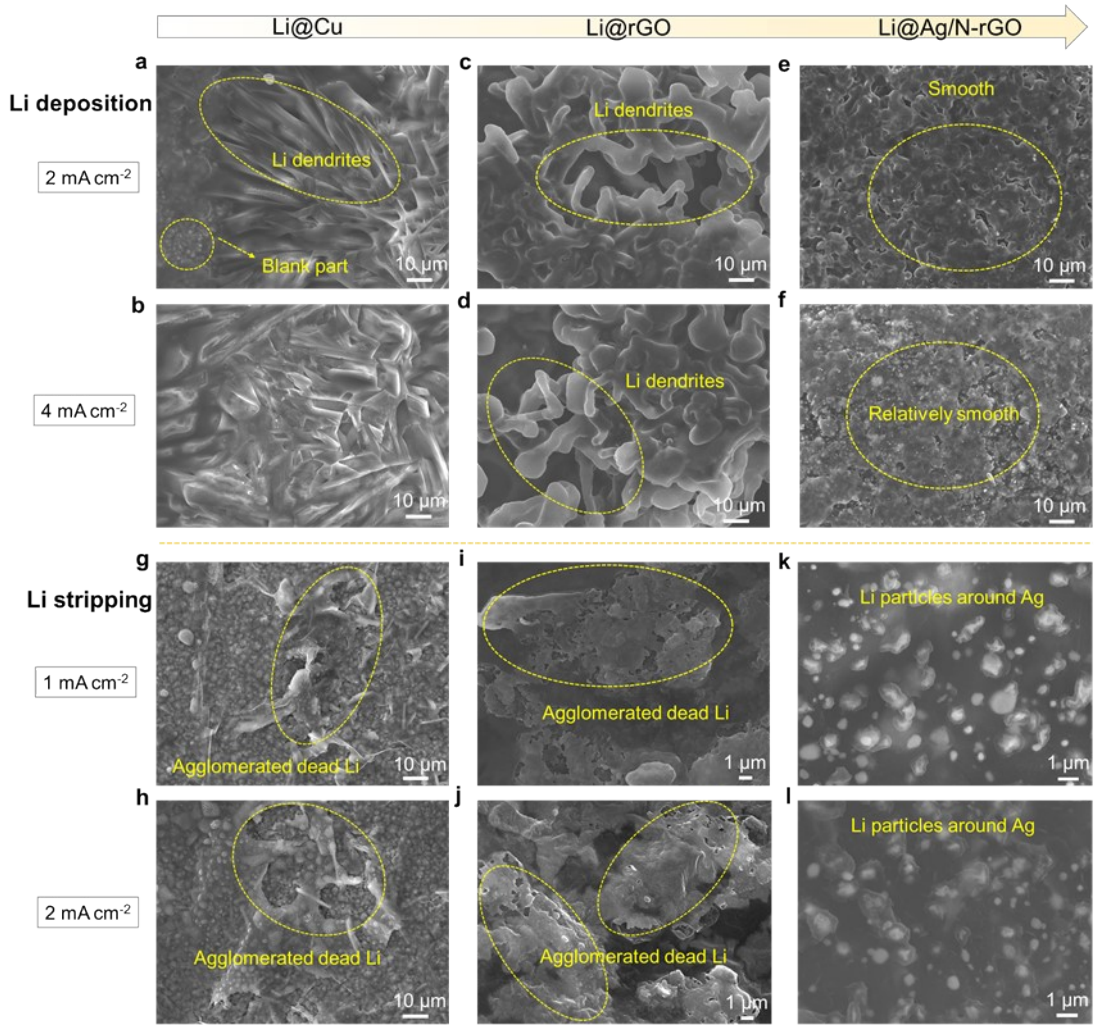

Fig. S15 Morphology of Li deposition/stripping behaviors at different current densities. SEM images of the Li deposition behavior at 2 and 4 mA cm^{-2} on (a, b) Cu, (c, d) rGO, and (e, f) Ag/N-rGO substrate with a capacity of 2 mAh cm^{-2}. SEM images of the Li stripping behaviors at 1 and 2 mA cm^{-2} on (g, h) Cu, (i, j) rGO, and (k, l) Ag/N-rGO substrate with a capacity of 1 mAh cm^{-2}.

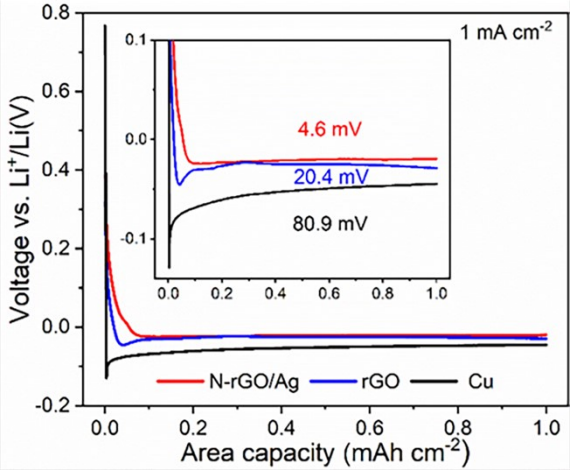

Fig. S16 Li deposition behavior of the Cu, rGO and Ag/N-rGO substrate. Voltage-capacity profiles of Li deposition for comparison of the nucleation overpotential at 1 mA cm^{-2}/1 mAh cm^{-2}.

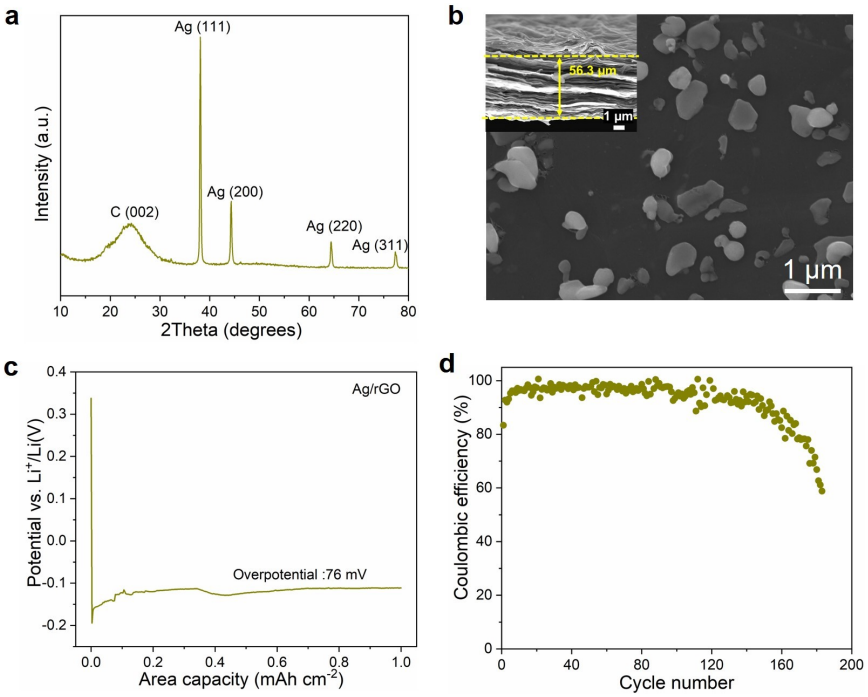

Fig. S17 Characterization and electrochemical performance of the Ag/rGO samples. (a) XRD patterns, (b) SEM images, (c) overpotential, and (d) CE of Ag/rGO electrode.

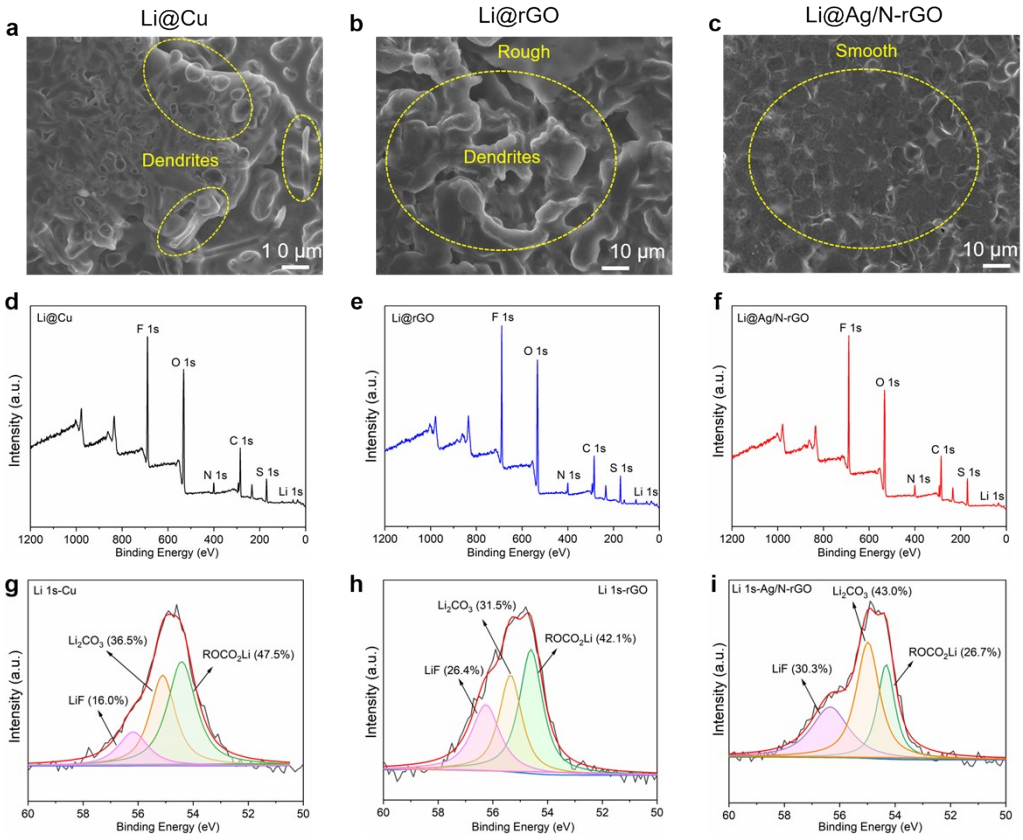

Fig. S18 Morphology and composition of cycled anode in full batteries. SEM images of the cycled Li anode on (a) Cu, (b) rGO, and (c) Ag/N-rGO substrate with a capacity of 3 mAh cm^{-2} at current density of 1 mA cm^{-2}. XPS full spectrum of (d) Cu, (e) rGO, and (f) Ag/N-rGO and Li 1s XPS spectra of (g) Cu, (h) rGO, and (i) Ag/N-rGO electrode in full cells after 40 cycles.

Table S1 Element contents of Ag/N-rGO.

Element	Atomic conc. (%)	Mass conc. (%)
Ag	1.9	14.8
C	86.6	73.1
O	5.6	6.3
N	5.8	5.7

Table S2 Comparison of cycling performance of Li@Ag/N-rGO symmetric cells in this work with a variety of previous reports.

Anode	Overpotential (mV)	Plating capacity (mAh cm^{-2})	Life span (h)	Reference
Ag@CMFs-Li	49	1	1000	[34]
Li-AgNP/CNF	25	1	500	[32]
Li-Co@N-rGO	10	1	1000	[25]
Li-rGO	~	1	222	[18]
N-rGO	22	0.042	<20	[30]
N,S-CDs	63	1	1200	[24]
Mg_xLi_y/LiF-Li-rGO	<40	1	450	[S1]
MXene/rGO-Li	36	1	500	[36]
3D Graphene	~	1	1000	[S2]
ZnSAs	12	1	800	[S3]
Li-SirGO	~	1	~100	[S4]
D-Ag@Li	~	1	>1300	[11]
Li@CGB	~	1	800	[14]
rGO-Ag-Li	25	1	200	[S5]
Li@Ag/N-rGO	6.8	1	1200	This work

Other Supplementary Material for this manuscript includes the following Video S1-S6:

Video S1 (.mp4 format) Li^+ concentration distributions with evolution mechanism of Li metal growth under unevenly distributed nucleation (Cu, rGO).

Video S2 (.mp4 format) Current density distributions with evolution mechanism of Li metal growth under unevenly distributed nucleation (Cu, rGO).

Video S3 (.mp4 format) Li^+ concentration distributions with evolution mechanism of Li metal growth under unevenly distributed nucleation (N-rGO).

Video S4 (.mp4 format) Current density distributions with evolution mechanism of Li metal growth under unevenly distributed nucleation (N-rGO).

Video S5 (.mp4 format) Li^+ concentration distributions with evolution mechanism of Li metal growth under uniformly distributed nucleation (Ag/N-rGO).

Video S6 (.mp4 format) Current density distributions with evolution mechanism of Li metal growth under uniformly distributed nucleation (Ag/N-rGO).

References

[S1] Q. Xu, X. Yang, M. Rao, D. Lin, K. Yan, R. A. Du, J. Xu, Y. Zhang, D. Ye, S. Yang, G. Zhou, Y. Lu, Y. Qiu, *Energy Storage Mater.* **2020**, *26*, 73.

[S2] L. Pan, Z. Luo, Y. Zhang, W. Chen, Z. Zhao, Y. Li, J. Wan, D. Yu, H. He, D. Wang, *ACS Appl. Mater. Interfaces* **2019**, *11*, 44383.

[S3] K. Xu, M. Zhu, X. Wu, J. Liang, Y. Liu, T. Zhang, Y. Zhu, Y. Qian, *Energy Storage Mater.* **2019**, *23*, 587.

[S4] H. Wang, X. Cao, H. Gu, Y. Liu, Y. Li, Z. Zhang, W. Huang, H. Wang, J. Wang, W. Xu, J. G. Zhang, Y. Cui, *ACS Nano* **2020**, *14*, 4601.

[S5] H. Zhuang, P. Zhao, Y. Xu, *Inorg. Chem. Front.* **2020**, *7*, 897.